09.1

Greenish white emission of ZnO microwalls fabricated by a hot target magnetron sputtering method

© A.P. Tarasov[1], A.M. Ismailov[2], A.E. Muslimov[1]

[1] Shubnikov Institute of Crystallography „Crystallography and Photonics“, Russian Academy of Sciences, Moscow, Russia
[2] Dagestan State University, Makhachkala, Dagestan Republic, Russia
E-mail: tarasov.a@crys.ras.ru

Received August 15, 2023
Revised September 9, 2023
Accepted September 13, 2023

The processes of formation of two-dimensional ZnO microstructures were studied for the first time using the hot magnetron sputtering regime. The fabricated microstructures had a morphology of multilayer walls $1-2\,\mu$m thick and were characterized by the presence of pores up to $10\,\mu$m in size. The UV-vis and photoluminescence spectroscopy methods revealed a significant modification of the optical properties of structures as a result of heat treatment. In particular, postgrowth annealing resulted in a significant enhancement of the narrow UV near-band-edge emission band, as well as the appearance of strong visible luminescence. A sufficiently long wavelength position (~ 545 nm) and a large width (FWHM ~ 140 nm) of the visible luminescence band cause the visually observed bright greenish white emission.

Keywords: zinc oxide, hot target, magnetron sputtering, 2D structures, microwalls, white luminescence, white light source.

DOI: 10.61011/TPL.2023.11.57197.19707

The rapid growth of world economy and depletion of energy reserves impose strict requirements on the energy efficiency of industrial equipment, devices, and instruments. Lighting equipment accounts for a considerable fraction of the overall power consumption. Traditional incandescent and fluorescent lamps were driven into the background after the invention of light-emitting diode (LED) devices. LEDs emitting in the blue region of the spectrum and luminophores absorbing blue quanta and converting them into lower-energy ones are the key components of so-called white LEDs [1,2]. Multilayer structures, which are typically based on InGaN/GaN, are used as blue LEDs. Individual layers in a multilayer structure may be strained; this affects the band structure parameters of InGaN and reduces the efficiency of luminophore excitation. Powders of complex compounds doped with rare-earth elements (e.g., YAG:Ce [3] and $Sr_3GdNa(PO_4)_3F$:Dy [4]) are commonly used as luminophores. The research into organic luminophores is also progressing rapidly at present [5–7]. In general, the concept of integration of a LED and a luminophore in a single package makes the fabrication technology more complex and reduces the product yield. The optimum way is to use a readily available and processable material with a wide emission spectrum in the visible region and a high light yield. The search for materials having these features and satisfying all the requirements for production is relevant at present. Wide-band semiconducting zinc oxide (ZnO) appears to be a promising research target in this context. Owing to its unique electrophysical and optical properties, relatively low cost, and the potential to produce a wide variety of micro- and nanostructures, this material is examined for various applications in optoelectronics and photonics [8].

The typical ZnO luminescence spectrum contains two major bands: a narrow near-band-luminescence band in the $380-390$ nm region and a relatively broad visible luminescence band, which is often characterized by a maximum in the green range ($490-530$ nm). At the same time, the examination of intrinsic defects in ZnO reveals a broad spectrum of potential radiative transitions that cover almost the entire visible range [9]. While on the subject of intrinsic defects, such transitions are associated mostly with oxygen (V_O) and zinc (V_{Zn}) vacancies, interstitial oxygen (O_i) and zinc (Zn_i) in various charge configurations, and their complexes. In this respect, the study of defects in ZnO and the processes of their production appears to be an instructive but challenging pursuit. The use of „hot“ magnetron sputtering from an uncooled target is one of the ways to produce a high defect density in ZnO [10]. Defect grain boundaries form in the regime of deposition of ZnO microclusters with a low diffusion activity. In addition, two-dimensional (2D) structures form with a high probability at the initial stages of growth under the conditions of suppressed lateral activity of ZnO microclusters. Two-dimensional structures (including ZnO-based ones) are being studied extensively due to their unique properties, which are attributable to a high surface-to-bulk ratio, porosity, etc. [11,12]. In the context of photonics, a well-developed morphology of 2D structures provides a high light yield due to an increase in the effective emitting area. Specifically, bright UV luminescence was reported for 2D ZnO nanostructures with the morphology of walls, sheets, combs, etc. [13–15]. Its brightness is

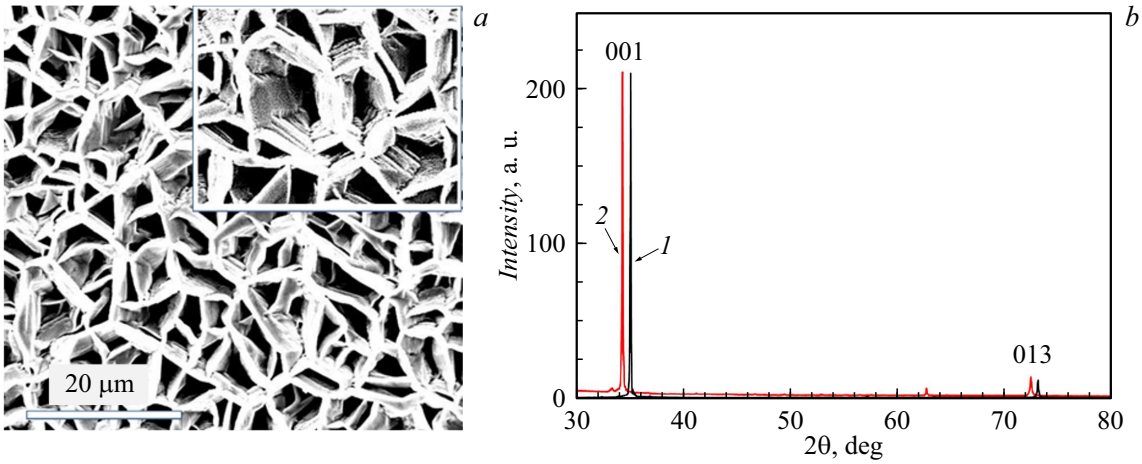

Figure 1. *a* — Electron microscopic image of the bottom surface of the ZnO film (from the substrate side); *b* — X-ray diffraction patterns recorded from the top (*1*) and bottom (*2*) sides of the ZnO film.

governed not by the morphology of crystals, but by their dimensionality (under equal synthesis conditions) [15]. A branched structure of arrays of 2D ZnO crystallites may provide feedback sufficient for excitation of stimulated emission and, in particular, random lasing [16,17]. In addition, the 2D morphology facilitates bulk and surface diffusion processes and may provide an opportunity to alter radically the luminescent properties of a structure through the use of thermal processing.

In the present study, the processes of formation of 2D ZnO microstructures on the *r*-plane of sapphire by magnetron sputtering of a hot target and their influence on the spectral features of ZnO in the near UV and visible ranges have been examined for the first time. The effect of thermal processing on the optical and emissive properties of the obtained microstructures has also been studied.

The *r*-plane of sapphire subjected to mechanochemical polishing was used as substrates. ZnO films were deposited by magnetron sputtering at a temperature of 750°C in the oxygen atmosphere under a pressure of 1.33 Pa with cooling excluded in accordance with the procedure outlined in [10]. The discharge current was 500 mA, and the deposition time was 35 min. Postgrowth annealing of ZnO films was performed in a tube furnace under the conditions of open air for 8 h at a temperature of 800°C.

X-ray diffraction (XRD) was used for structural studies of films. X-ray patterns were recorded with an Empyrean (PANalytical, Netherlands) diffractometer in the Bragg–Brentano geometry. Copper anode radiation ($CuK_{\alpha 2} = 1.54$ Å) was used. The High Score Plus software and the ICSD (PDF-2) database were used to analyze the diffraction patterns and identify peaks. Electron microscopic studies of a transversely cleaved sample were carried out with a Jeol Neoscope 2 (JCM-6000) scanning electron microscope.

The photoluminescence (PL) of samples was examined under excitation by the third harmonic (355 nm) of a pulsed Nd:YAG laser. The pulse width and repetition rate were 10 ns and 15 Hz, respectively. The photoexcitation power density on the sample surface was ~ 0.1 MW/cm^2 (the laser spot diameter at the sample was $\sim 200\,\mu$m). An MDR-206 monochromator coupled with a „Videoskan“ CCD camera were used to record the PL spectra of samples. Total transmittance spectra were recorded by a SPECORD 200 PLUS double-beam spectrophotometer fitted with an integrating sphere. All measurements were performed at room temperature.

According to electron microscopy data, the thickness of the ZnO film on the *r*-plane of sapphire was 53 μm. The mean ZnO film growth rate was on the order of 1.51 μm/min, which is a high value comparable to the rate of growth of uniaxial ZnO microcrystals. This rate was achieved owing to the emission of clusters [10] from the overheated target surface and their incorporation into the growing ZnO film. The ZnO film surface was rough and morphologically uniform.

At the next stage, the ZnO film was separated mechanically from the sapphire substrate. A significant (more than 10-fold) difference between the thermal expansion coefficients of ZnO and sapphire and a fairly large thickness of the film facilitated this process. According to electron microscopy data, the bottom (back) film surface (Fig. 1, *a*), which was adjacent to the substrate surface in the course of growth, differed radically from the top (free) surface. The bottom surface was a honeycomb-like structure with pores 3–10 μm in linear size and up to 5 μm in depth. Since the pore wall thickness was 1–2 μm, they could be regarded as microwalls. A multilayer wall structure was observed. A similar pattern of layer-by-layer growth was also reported in studies into ZnO nanowall formation on the *r*-plane of sapphire by gas-transport synthesis [17]. According to XRD data (Fig. 1, *b*), both sides of the ZnO film were textured along the [0001] direction. The XRD curve recorded from the back side of the film featured additional

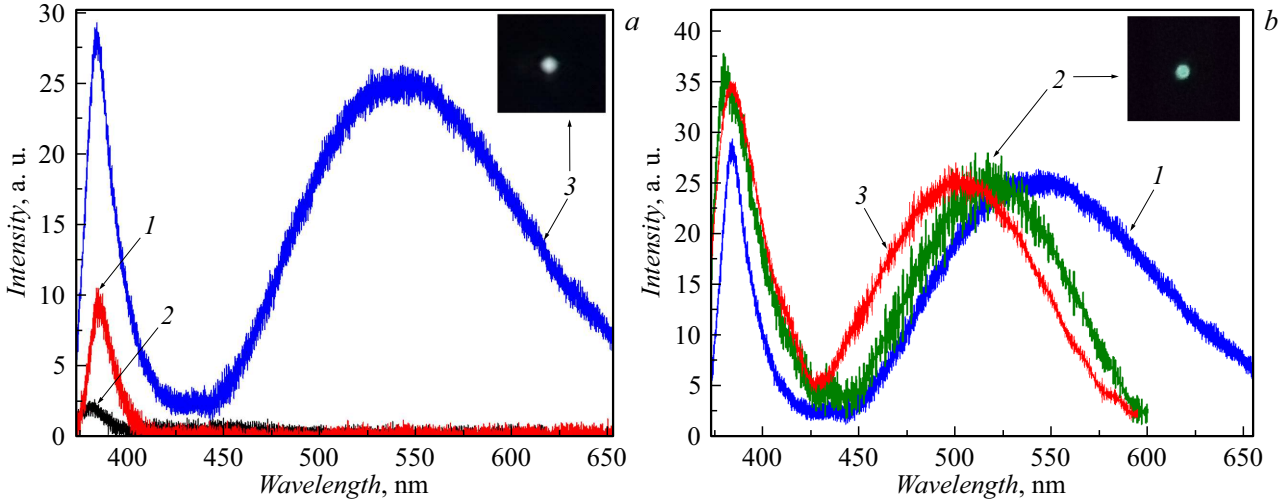

Figure 2. *a* — PL spectra of the ZnO film. *1* — Bottom side prior to annealing, *2* — top side after annealing, and *3* — bottom side after annealing (photographic image of the emitting film is shown in the inset). *b* — PL spectra of various ZnO structures. *1* — ZnO film examined in the present study (bottom side after annealing), *2* — ZnO microcrystals produced using the modified thermal evaporation method (photographic image of emitting microcrystals is shown in the inset), and *3* — ZnO film fabricated by gas-transport synthesis.

reflections associated with parasitic [013] crystallites. The ZnO lattice constants determined based on XRD data for one side of the film differed significantly from those corresponding to the other side. Parameters $d_{001} = 2.61$ Å and $d_{013} = 1.48$ Å for the porous film part were close to the standard ones ($d_{001} = 2.60$ Åand $d_{013} = 1.477$ Å). At the same time, parameter $d_{001} = 2.56$ Å for the top film side was more than 1% smaller than the standard one. This corresponds to a stress on the order of 2%.

The PL spectra of the film (Fig. 2, *a*) confirm that the bottom side was of a higher quality than the top side. Specifically, prior to thermal processing, the signal from the top film side was too weak to record a spectrum with an acceptable signal-to-noise ratio at the excitation level set in experiments. PL from the bottom film side was, on the contrary, easy to detect (curve *1* in Fig. 2, *a*). This PL was represented by just a narrow near-band-luminescence band of ZnO with its maximum at 385 nm and a full width at half maximum (FWHM) of 15 nm; no visible radiation was detected.

Postgrowth processing improved the optical quality of the film, exerting a significant effect on its PL spectrum. An near-band-luminescence band with an intensity sufficient for its reliable detection (curve *2* in Fig. 2, *a*) was revealed on the top film side after annealing. In addition, a weak band in the blue region with a maximum around 450 nm also became visible. The PL recorded from the back film side intensified significantly (curve *3* in Fig. 2, *a*). Specifically, the near-band-luminescence band intensity increased by a factor of more than 3. The most striking change, however, was the emergence of a visible luminescence band with a considerable intensity that formed the major part of emission. Its maximum was at a wavelength of ~ 545 nm, and the FWHM was ~ 140 nm (0.58 eV); thus, this band occupied the entire green and yellow regions of the spectrum and certain parts of the blue and red regions. Positioned at relatively long wavelengths and having a considerable FWHM, this band accounted for the observation of bright white emission with a greenish tint (see the inset in Fig. 2, *a*).

PL spectra of the examined film after annealing (curve *1*), ZnO microcrystals (similar to those studied in [18,19]) grown using the modified thermal evaporation method (curve *2*), and the ZnO microfilm fabricated by gas-transport synthesis [20] (curve *3*) are shown for comparison in Fig. 2, *b*. For ease of comparison, these spectra are normalized to the maximum of the visible emission component. Under similar excitation conditions, the microfilm and microcrystals also reveal two luminescence bands: near-band-luminescence and visible radiation. However, compared to the examined film, these structures had a significantly (~ 1.4-fold) lower FWHM of the visible emission band, and the band itself was position at shorter wavelengths (its maximum corresponded to $\sim 500-515$ nm). Therefore, the visible emission of these structures is greenish-blue (see the inset in Fig. 2, *b*) with a blue tint provided partially by the fairly broad (FWHM $\sim 28-30$ nm) near-band-luminescence band, which occupies a certain part of the blue spectral region. Figure 3, *a* presents the chromatic diagram plotted in accordance with the International Commission on Illumination (CIE) standard of 1931. Color points corresponding to the PL data of the examined film and microcrystals (see spectra *1* and *2* in Fig. 2, *b*) are indicated. Chromatic coordinates for the film were $x = 0.362$, $y = 0.488$.

The emergence of visible emission from the back film side after thermal processing is apparently attributable not only to defect diffusion in its structure and active formation of V_O-type defects, but also to the deactivation of absorption

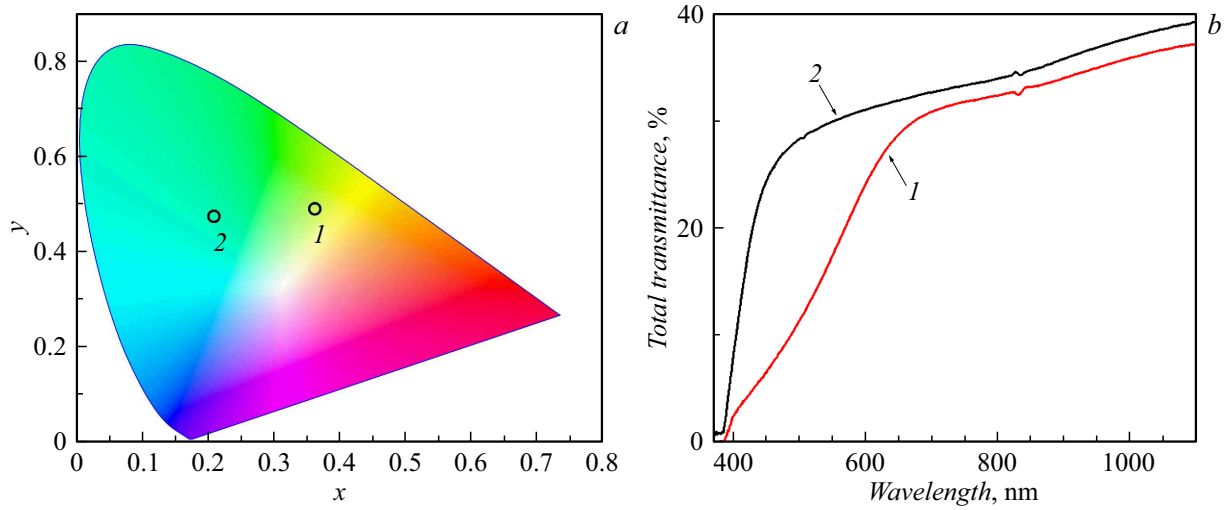

Figure 3. *a* — Color points corresponding to the emission of the ZnO film (point *1*, which corresponds to curve *1* in Fig. 2, *b*) and ZnO microcrystals (point *2*, which corresponds to curve *2* in Fig. 2, *b*) on the CIE1931 chromatic diagram. A color version of the figure is provided in the online version of the paper. *b* — Total transmittance spectra of the ZnO film recorded before (*1*) and after (*2*) thermal processing.

centers for visible radiation. This is evidenced by the results of comparison of the total transmittance spectra of the film recorded before and after annealing (Fig. 3, *b*). Specifically, the transmittance spectrum of the film prior to annealing (curve *1* in Fig. 3, *b*) contains a broad absorption band (located approximately within the 400–650 nm interval). This explains why no visible luminescence was observed and why the film had a brownish-orange color. The transmittance of the film in the visible range increased considerably after annealing (curve *2* in Fig. 3, *b*). On visual inspection, the film appeared much lightr and acquired a gray-green color.

We note in conclusion that the obtained ZnO structure may serve as a basis for further research aimed at fabricating a white light source. The color tint of emission of such a device may presumably be adjusted and controlled by altering the postgrowth processing conditions, introducing impurities in the course of growth, and forming hybrid ZnO-based materials.

Acknowledgments

The authors wish to thank I.D. Venevtsev for his help in the examination of films.

Funding

The synthesis of samples was carried out under the state assignment of FSRC „Crystallography and Photonics“ of the Russian Academy of Sciences, and the examination of their structural and optical properties was supported by grant MK-3140.2022.1.2 from the President of the Russian Federation.

Conflict of interest

The authors declare that they have no conflict of interest.

References

[1] E.-M. Bourim, J.I. Han, Electron. Mater. Lett., **11** (6), 982 (2015). DOI: 10.1007/s13391-015-5180-0
[2] I.-W. Cho, B. Lee, M.-Y. Ryu, K. Lee, J.S. Kim, J. Korean Phys. Soc., **78** (4), 275 (2021). DOI: 10.1007/s40042-020-00041-7
[3] A.C. Berends, M.A. van de Haar, M.R. Krames, Chem. Rev., **120** (24), 13461 (2020). DOI: 10.1021/acs.chemrev.0c00618
[4] L. Han, Y. Sun, J. Sun, J. Rare Earths, **34** (1), 12 (2016). DOI: 10.1016/s1002-0721(14)60571-8
[5] G.M. Farinola, R. Ragni, Chem. Soc. Rev., **40** (7), 3467 (2011). DOI: 10.1039/c0cs00204f
[6] W.-Y. Wong, C.-L. Ho, J. Mater. Chem., **19** (26), 4457 (2009). DOI: 10.1039/b819943d
[7] S. Mukherjee, P. Thilagar, Dyes Pigm., **110**, 2 (2014). DOI: 10.1016/j.dyepig.2014.05.031
[8] J. Rodrigues, N.B. Sedrine, M.R. Correia, T. Monteiro, Mater. Today Chem., **16**, 100243 (2020). DOI: 10.1016/j.mtchem.2020.100243
[9] A. Galdámez-Martinez, G. Santana, F. Güell, P.R. Martínez-Alanis, A. Dutt, Nanomaterials, **10** (5), 857 (2020). DOI: 10.3390/nano10050857
[10] A.M. Ismailov, V.A. Nikitenko, M.R. Rabadanov, L.L. Emiraslanova, I.S. Aliev, M.K. Rabadanov, Vacuum, **168**, 108854 (2019). DOI: 10.1016/j.vacuum.2019.108854
[11] S.-W. Kim, H.-K. Park, M.-S. Yi, N.-M. Park, J.-H. Park, S.-H. Kim, S.-L. Maeng, C.-J. Choi, S.-E. Moon, Appl. Phys. Lett., **90** (3), 033107 (2007). DOI: 10.1063/1.2430918
[12] C. Li, L. Yu, X. Fan, M. Yin, N. Nan, L. Cui, S. Ma, Y. Li, B. Zhang, RSC Adv., **10** (6), 3319 (2020). DOI: 10.1039/c9ra07933e

[13] A. Pan, R. Yu, S. Xie, Z. Zhang, C. Jin, J. Cryst. Growth, **282** (1), 165 (2005). DOI: 10.1016/j.jcrysgro.2005.05.003
[14] M.M. Brewster, M.Y. Lu, S.K. Lim, M.J. Smith, X. Zhou, S. Gradecak, J. Phys. Chem. Lett., **2** (15), 1940 (2011). DOI: 10.1021/jz2008775
[15] A.P. Tarasov, L.A. Zadorozhnaya, B.V. Nabatov, I.S. Volchkov, V.M. Kanevsky, Cryst. Rep., **68** (2), 293 (2023). DOI: 10.1134/S1063774523020190.
[16] L. Miao, S. Tanemura, H.Y. Yang, S.P. Lau, Int. J. Nanotechnol., **6** (7-8), 723 (2009). DOI: 10.1504/IJNT.2009.02531
[17] A.P. Tarasov, C.M. Briskina, V.M. Markushev, L.A. Zadorozhnaya, I.S. Volchkov, Opt. Mater., **102**, 109823 (2020). DOI: 10.1016/j.optmat.2020.109823
[18] A.P. Tarasov, A.S. Lavrikov, L.A. Zadorozhnaya, V.M. Kanevsky, JETP Lett., **115** (9), 502 (2022). DOI: 10.1134/S0021364022100514.
[19] A.P. Tarasov, A.E. Muslimov, V.M. Kanevsky, Materials, **15** (24), 8723 (2022). DOI: 10.3390/ma15248723
[20] L.A. Zadorozhnaya, A.P. Tarasov, I.S. Volchkov, A.E. Muslimov, V.M. Kanevsky, Materials, **15** (22), 8165 (2022). DOI: 10.3390/ma15228165

Translated by D.Safin